IFSCC 2025 full paper (IFSCC2025-783)

World's thickest 'close to real life' artificial human skin with muscle, hypodermis, dermis and epidermis for modelling of ageing skin, wrinkles and cosmetics development.

Clément Milet[1], Alizé Vialle[1], Anne-Laure Desroches[1], Pauline Payen[1], Mathieu Lacroix[1], Tiffany Luangvannasy[1], Niels Loulier[1], Nico Forraz[1], Colin McGuckin[1*],

1 CTISKIN, CTIBIOTECH, Meyzieu, France

* Colin McGuckin, CTIBIOTECH™, Bat A16, 5 Avenue Lionel Terray, Meyzieu-LYON, France. +33967107455, c.mcguckin@ctibiotech.com

1. Introduction

Skin ageing is a multifactorial biological process that affects the structural and functional integrity of all skin layers [1]. Clinically, it is characterised by the appearance of fine lines, wrinkles, a certain loss of elasticity and changes in pigmentation. At a tissue level, these symptoms are the result of combined changes to the epidermis, dermis, hypodermis and underlying subcutaneous muscular layer [2]. More specifically, thinning of the epidermis results in an altered barrier function and delayed healing; degradation of the dermal matrix, particularly collagen and elastin, contributes to reduced mechanical strength and elasticity; loss of adipose tissue in the hypodermis alters the volume and contour of the skin, and muscle atrophy further exacerbates sagging and wrinkling by weakening the structural support of the overlying tissues.

Although significant advances have been made in dermatological research and tissue engineering, current in vitro models of human skin are mainly limited to the reconstruction of partial skin equivalents, generally including only the epidermal and dermal layers [3]. These simplified models fail to reproduce the complex multilayered architecture of native human skin, and are insufficient to study complex processes such as aging, inflammation, vascularization or the impact of mechanical stress. Furthermore, the absence of deeper layers such as hypodermis and muscle also limits the relevance of these models for applications in cosmetic testing and drug delivery.

To overcome these limitations, we have developed a new, full-thickness, multilayered in vitro human skin model that closely mimics the functional characteristics of native skin. Our 3D models incorporates the four main skin compartments: a stratified epidermis, a dermis composed of both fibroblasts and M1 macrophages, a biologically active adipose layer and a functional layer of muscle tissue. The model is designed to be modular and adaptable, allowing the inclusion of additional physiological components such as various immune cells and microvascular networks [4] [5], enabling more comprehensive research into skin biology under normal and pathological conditions.

Our model represents a significant advance in skin tissue engineering by providing a flexible, physiologically relevant testing tool to study age-related changes, immune interactions and therapeutic interventions in a realistic human skin microenvironment.

2. Materials and Methods

2.1. Sample collection

Skin samples and buffy coat sample were obtained from human biological samples following informed consent and applicable French and European ethical guidelines and regulations from local hospitals in Lyon, France.

2.2. Cell isolation and amplification

Fibroblasts and Keratinocytes were isolated from human skin donors using enzymatic dissociation and grown in 6-well plates (Corning) using RPMI 1640 medium (HyClone, Cytiva) supplemented with 15% FBS (HyClone), ciprofloxacin (4 µg/ml) and EpiLife medium (Gibco, Life Technologies, France) supplemented with Human Keratinocytes Growth Supplement (HKGS, Gibco, Life Technologies, France) respectively.

Adipocytes were isolated from hypodermis of human skin samples and grown in 6-well plates (Corning) using collagen coating and proprietary medium CTIGM.Adipocytes Growth medium (CTIBiotech, France).

Myocytes were obtained from normal muscle samples, amplified in culture using Ham's F-10 GlutaMAX (Gibco) supplemented with 15% FBS and secondly isolated using immunomagnetic isolation before immunofluorescent staining of desmin to confirm purity of cell populations.

Peripheral blood mononuclear cells (PBMC) were first isolated from buffy coat using Ficoll-Paque Plus (Cytiva, France) and counted on a LUNA-FL dual fluorescence cell counter (Logos Biosystems, France). Then, CD14+ monocytes were positively selected and isolated following CD14+ MicroBeads kit (Miltenyi Biotec, France). To verify the performance of the kit and ensure good isolation of CD14+ monocytes, flow cytometry was performed using a BD FACSVerse flow cytometer (BD Biosciences, France). During the entire isolation process, the viability of all cells was tested using a LUNA-FL fluorescence cell counter.

2.3. Bioinks preparation

After amplification in 225 cm^2 flasks, fibroblasts, keratinocytes and adipocytes were harvested with Tryple Select enzyme (Life Technologies, France) before centrifugation. CD14+ monocytes and myocytes were thawed in water bath at 37°C and resuspended in warm PBS before centrifugation. All the cells were counted using a LUNA-FL fluorescence cell counter.

CD14+ monocytes and fibroblasts were mixed together with a specific bioink allowing the cells to grow and spread (Cellink, Sweden) to create the dermis immune layer. Adipocytes were mixed separately with a second bioink (Cellink) to create the hypodermis layer and finaly myocytes were mixed separately with a third bioink (Cellink) to create the muscle layer. Bioinks containing cells were then placed into 3 separate 3 ml cartridges (Optimum EFD, Nordson, USA).

2.4. 3D Bioprinting

First, 3D models were separately designed using a open-source computer-aided design software (Prusa Slicer) to create 3D models for immune dermis, hypodermis and muscle layers. 3D models were then combined to prepare the final G-code file after slicing in Prusa Slicer,

based on open-source Slic3r software. The G-code file, containing positions and trajectories instructions, was transferred to a USB drive and connected to a BIO X Bioprinter (Cellink). The 3D bioprinting process was performed under sterile conditions, under a laminar flow hood to avoid contamination.

The cartridges containing the bioinks were placed in the defined print heads, the bioprinter calibrated, the G-code selected and the models 3D bioprinted in 12-well plates according to our standard procedure.

2.5. Maturation in culture

Directly after 3D bioprinting, 3D models were crosslinked using $CaCl_2$-containing Crosslinking Agent and thrombin for 5 minutes according to the supplier protocol (Cellink). The 3D models were then rinsed on time with PBS 1X (Corning).

3D printed models were grown for 31 days in Transwell culture inserts (VWR, USA), including the stages of dermal maturation, M1 macrophages differentiation, epidermal differentiation, air-liquid interface and cornification of the bioprinted models.

2.6. Viability analysis

Every 5 to 7 days, 3D models were analyzed to evaluate viability and morphology of the cells inside the 3D models. Specific kit of viability, Live/Dead reagents (Invitrogen, USA) was used. Calcein AM (live cells) and Ethidium homodimer-1 (dead cells) for 30 minutes before microscopic analysis. Live cells were analyzed at 494/517 nm and dead cells at 528/617 nm (excitation/emission) on an inverted fluorescence microscope (Ti-S Eclipse, NIKON, Japan).

2.7. Viability quantification

Medium supplemented with 10% of AlamarBlue Cell Viability reagent (Invitrogen, USA) was directly added in each individual 3D models well and incubated for 4 hours. At the end of incubation, cell culture supernatants were collected and transferred to a black-walled 96-well plate. Fluorescence was quantified on a microplate reader (Tecan Spark) at 550 nm, excitation and 590 nm, emission.

2.8. Analysis of lipid droplet production

After fixation with formaldehyde 4% w/v (Sigma-Aldrich), and 3 successive rinsing in PBS 1X, 3D models were stained with 7 µg/ml Nile Red (Sigma-Aldrich) and 2 µg/ml 4',6-diamidino-2-phenylindole (DAPI, Sigma-Aldrich) overnight before microscopic analysis.

Total lipids were analyzed at 520/625 nm, neutral lipids at 475/530 nm and nuclei at 356/465 nm (excitation/emission) on an inverted fluorescence microscope (Ti-S Eclipse, NIKON).

2.9. Injection of formulation

The 3D models were injected with either a control solution (PBS), lipopolysaccharide (LPS, 5 µg/ml), or mRNA formulations (mRNA 1 & 2) to simulate immune system activation. To ensure consistent and precise administration of the formulations, a BIO X Bioprinter (Cellink) was used to accurately position a Hamilton syringe equipped with a 27-gauge needle into the muscle layer of the 3D models. A volume of 15 µl of each formulation was then manually injected.

2.10. Pro-inflammatory cytokines dosage

Following maturation and treatment steps, supernatants were collected 24, 48 and 72 hours after injection of formulation. Dosage of cytokines was performed using BD Cytometric Bead Array (CBA) kit from on BD FACSVerse flow cytometer. This kit allowed the simultaneously analysis of IL-1α, IL-1β, IL-6, IL-8, INFy and IL-10.

2.11. Histology

At the end of the experiment, 3D models were rinsed once with PBS 1X (Corning) and fixed in formaldehyde 4% w/v (Sigma-Aldrich), before dehydration in alcohol crescent baths and clarification in xylene. Samples were then embedded in paraffin and sectioned into 5 µm thick slices. After rehydration process, slices were either directly coloured with hematoxylin, eosin and saffron (HES), or a heat-induced antigen retrieval step before immunohistochemical staining of myogenin and vimentin or CD68 and counterstaining of nuclei with DAPI.

3. Results

3.1. Production of models using 3D Bioprinting technology

First, we created the 3D model using computer-aided design software. This step defines the future three-dimensional organization to be used by the 3D bio-printer. All the layers including muscle, fat, dermis are first designed individually, then combine together to be precisely positioned in a final design (Figure 1a).

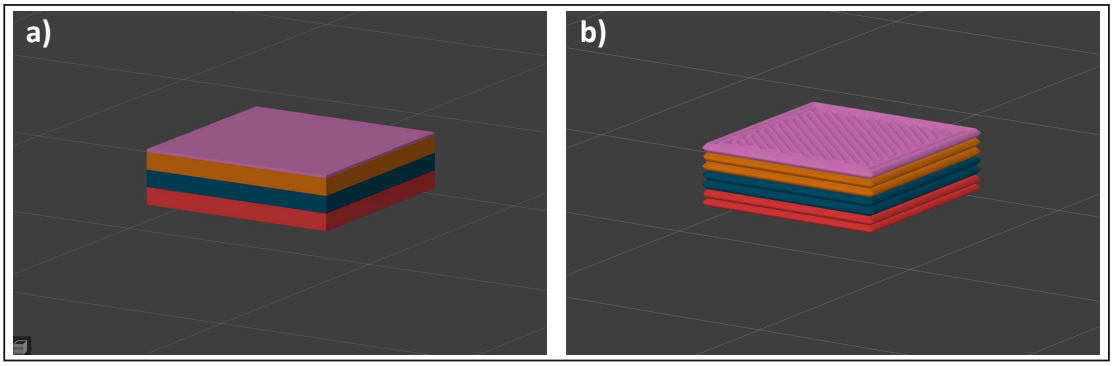

Figure 1. Design of the 3D models using computer-aided design software (Prusa Slicer): (a) Combining of all the layers into the designing software (b) Slicing of the model to create G-code file containing layers, positions and trajectories instructions.

As with any additive manufacturing project, the final design was sliced to create a G-code, a file containing the instructions and trajectories that will be transmitted to the 3D bio-printer throught a USB drive (Figure 1).

3D models were grown in Transwell culture inserts as described previously [5] for 31 days after bioprinting and cell viability was assessed using Live/Dead staining at day 31 (Figure 2).

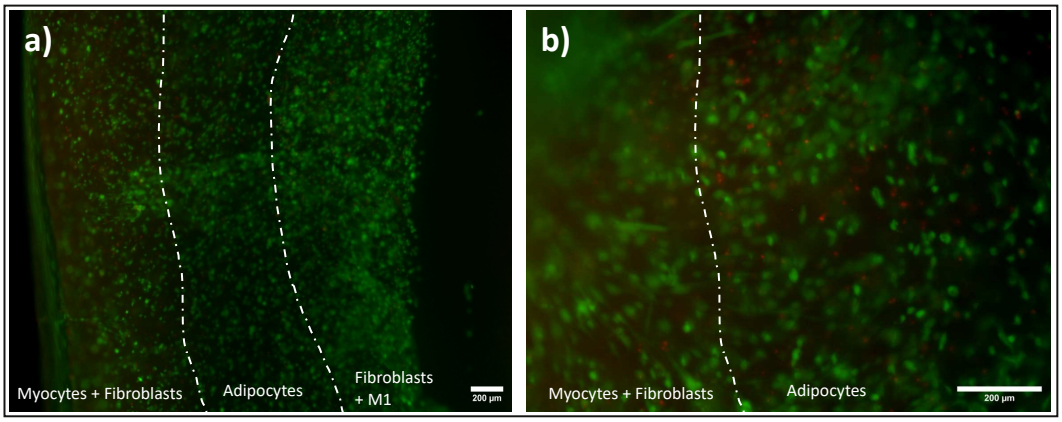

Figure 2. *Fluorescence imaging after Live/Dead staining of 3D bioprinted models. Imaging was performed at the end of the maturation phase.* Live cells stained in green and dead cells in red. *a) 4X magnification imaging; b)* 20X magnification imaging.

Cell viability within the bioinks was confirmed to be very high for all the different cell types in all layers, with only a few dead cells observed 31 days after bioprinting. This highlights the suitability of the bioinks selected. In addition, the 3D morphology of the cells inside the bioinks was clearly maintained (Figure 2a).

3.2. A functionnal 3D Bioprinted complex skin model

a. Hypodermal layer

To assess the structural integrity and functional viability of the adipocytes integrated into the bioink, we evaluated their capacity to accumulate lipids, a characteristic of mature, metabolically active adipocytes. Staining with Nile Red, a fluorescent dye specific for lipids, was performed on the 3D models 31 days after 3D bioprinting. After staining, the samples were imaged using a fluorescence microscope. Analysis revealed the presence of well-defined lipid droplets in the cytoplasm of cells dispersed in the models, indicating successful adipogenic differentiation and maintenance of adipocyte functionality in the 3D environment (Figure 3). The spatial distribution and intensity of lipid staining further suggest that the bioink composition and printing process did not compromise adipocyte morphology or function, confirming its suitability for modelling adipose tissue *in vitro*.

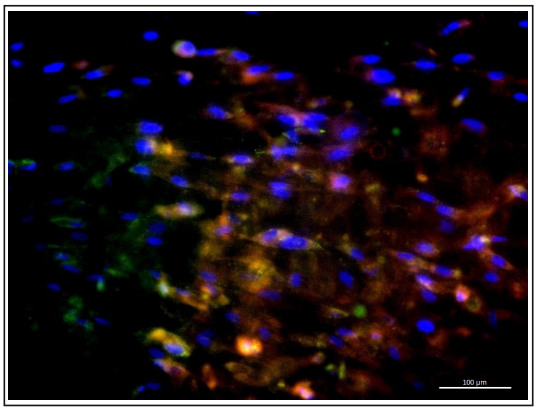

Figure 3. *Fluorescence imaging of 3D bioprinted models following Nile Red staining of lipid droplets.* Total lipids stained in red, neutral lipids in green, lipids droplets appears in yellow and nuclei appear in blue.

b. Muscular layer

The differentiation capacity of myocytes in the bioink after 3D bioprinting was evaluated. Immunohistochemical staining was performed targeting key markers of myoblasts differentiation. Specifically, the expression of myogenin, a transcription factor involved in the terminal differentiation of myoblasts, and vimentin, an intermediate filament protein associated with mesenchymal cells including fibroblasts, was assessed (Figure 4).

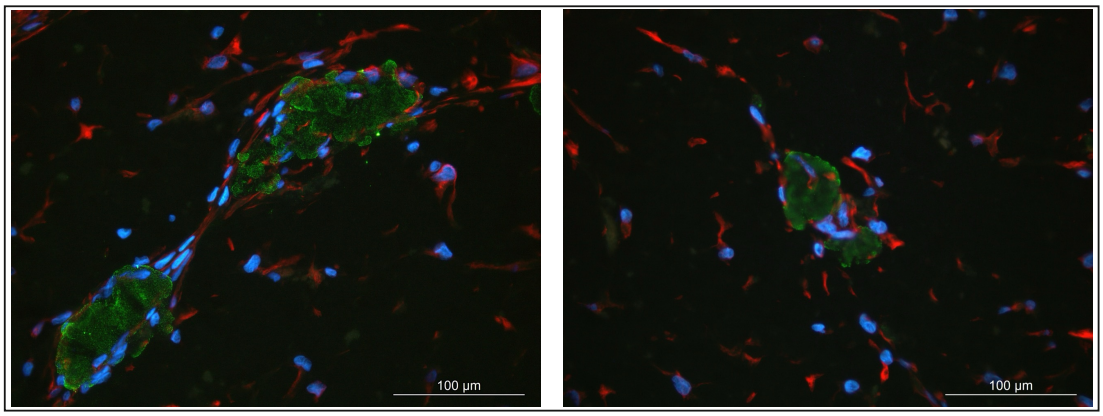

Figure 4. Fluorescence imaging after Myogenin (green) and Vimentin (red) and nuclei (blue) staining of 3D bioprinted models (x40 magnification).

Nuclear staining was also performed to visualise the distribution and morphology of the cells in the 3D models. These analyses enabled the identification and localisation of differentiated myocytes in the 3D bioprinted models, providing insight into the ability of the bioink to support the progression of the myogenic differentiaion in a 3D environment.

c. Immune, dermal and epidermal layer

Histological analysis was performed on paraffin sections of the 3D bioprinted complex skin model. This histological analysis enabled the tissue architecture to be assessed and the presence of immune cells within the construct to be confirmed. Staining with haematoxylin , eosin and saffron (HES) revealed a good distribution of fibroblasts in the dermis ink, as well as a multi-layered, differentiated and cornified yet thin epidermis. The dermal-epidermal junction (DEJ) is defined, separating the keratinocytes from the fibroblasts (Figure 5a).

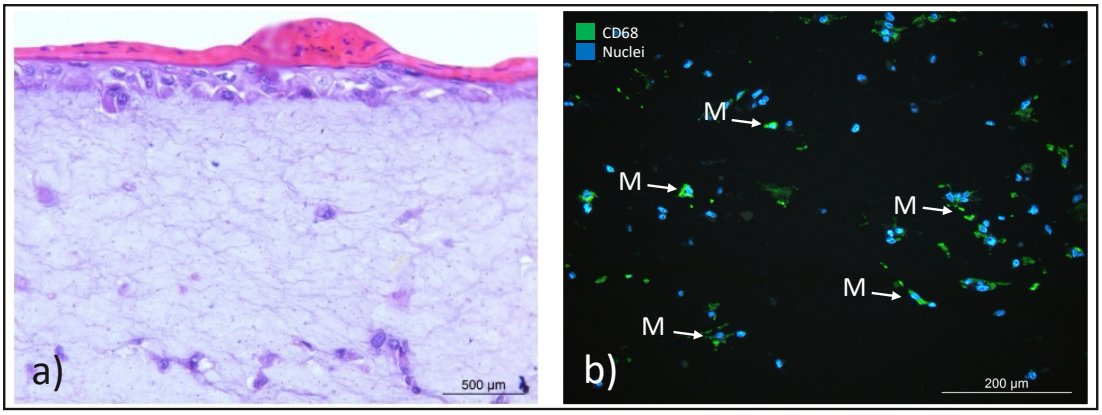

Figure 5. *Histology stainings after paraffin embedding of 3D bioprinted complex skin model including M1 macrophages.* a) HES staining to observe the morphology of the 3D models; b) Immunohistostaining of CD68 was performed to highlight M1 macrophages (green = CD68; blue = DAPI).

To specifically identify and locate M1 macrophages, immunohistochemical staining targeting CD68, a pan-macrophage marker was used. CD68-positive cells were visualised using a fluorescent secondary antibody (green) and the nuclei were counterstained with DAPI (blue), allowing precise spatial localisation of the macrophages in the tissue (Figure 5b). This staining confirmed the successful integration and persistence of M1 macrophages in the bioprinted model, confirming its relevance for the study of immune responses in modified human skin.

3.3. Semi-automated injection of formulations

To ensure standardised and reproducible delivery of formulations into the muscle layer of 3-dimensional bioprinted models, a dedicated facility using a 3D bioprinter was set up. BIO X Bioprinter (CELLINK) was used to achieve precise spatial control during the injection process (Figure 6a). A Hamilton syringe fitted with a 27-gauge needle was mounted on the extrusion head of the bioprinter, allowing precise positioning in the desired depth of the 3D model (Figure 6b).

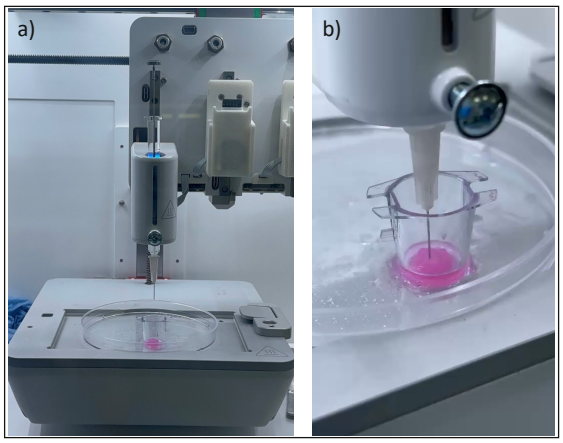

Figure 6. *3D bioprinter setup for calibrated injection of formulations in the muscle layer of 3D Bioprinted models.* a) Precise positioning of Hamilton syringe and 27-gauge needle; b) Injection of formulations in 3D models.

This configuration allowed the muscle-equivalent area of the construct to be consistently targeted, minimising variability in injection depth and location between samples. Next, a defined volume (15 µl) of each formulation, whether control, immunostimulatory or therapeutic, was manually injected under the guidance of the bioprinter (Figure 6b). This approach ensured both mechanical stability during injection and high reproducibility, which is essential for comparative analyses of biological responses under different experimental conditions.

3.4. Evaluation of metabolic activity

AlamarBlue assay, a non-toxic cell viability assay was performed at the start of the study and after 72 hours of treatment to evaluate the impact of different treatments on cell viability and metabolic function within 3D bioprinted structures. Metabolic activity was quantified based on the reduction of resazurin to resorufin by metabolic active and viable cells, and the results were normalised relative to the untreated control, set at 100% (Figure 7).

The PBS control group showed no significant variation in metabolic activity compared to the untreated control, indicating that the injection procedure and vehicle had no cytotoxic effect.

In contrast, lipopolysaccharide (LPS) treatment resulted in a slight increase in metabolic activity at 72 hours. However, this modest effect may underestimate the total biological response, as LPS is known to act rapidly via innate immune pathways, and its effects may have peaked before the 72-hour time point.

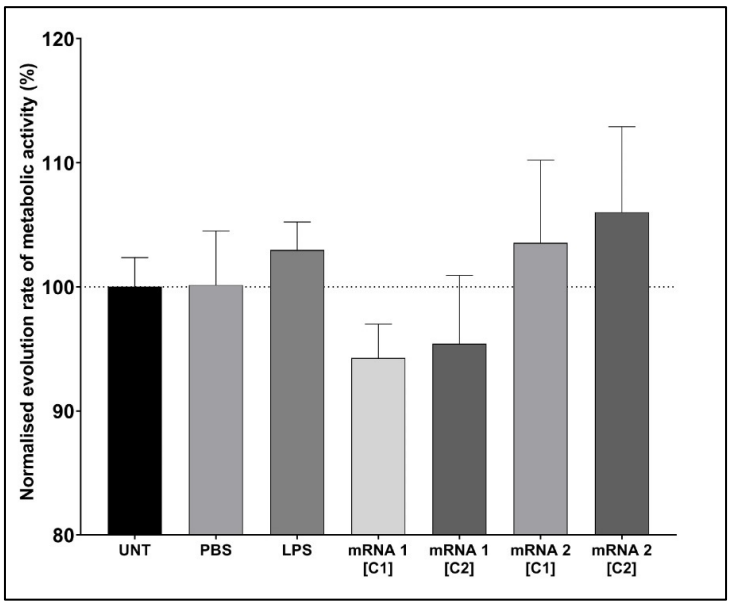

Figure 7. *Evolution rate of metabolic activity by AlamarBlue assay*. Comparison before and after 72 hours of treatment. The evolution rate has been normalised to the untreated control.

It is interesting to note that different responses were observed after treatment with the mRNA formulations. Administration of mRNA 1 at both tested concentrations resulted in a decrease in metabolic activity, suggesting a potential cytotoxic or inhibitory effect on cell function.

In contrast, treatment with mRNA 2 induced an increase in metabolic activity at both tested concentrations, indicating a possible stimulatory effect on cell viability or metabolism.

These results highlight distinct cellular responses to different mRNA constructs and underscore the importance of further mechanistic studies to elucidate their specific modes of action in complex tissue environments.

3.5. Inflammatory cytokines

Supernatants were collected 24, 48 and 72 hours after injection of controls or mRNA formulations and IL-10, IL-6, IL-8 and IL-1 β were quantified with CBA kit, and the results were normalised relative to the untreated control, set at 100% (Figure 8).

Firstly, analysis of IL-1β production shows a response exclusively at 48 hours, which is similar for the LPS control and for mRNA 1 C1, indicating a response to inflammation. mRNA 2 showed no change in IL-1β production (Figure 8a).

As expected, LPS induced a slight increase in IL-6 expression at 24 hours and 48 hours, followed by a decrease at 72 hours, reflecting a typical early-phase inflammatory response (Figure 8b). It should be noted that treatment with mRNA 1, particularly at concentration C1, also triggered a pronounced upregulation of IL-6 at 24 hours, similar to the LPS control, which then continued to increase, indicating significant inflammatory stimulation. In contrast, mRNA 2 caused only a modest and short-lived IL-6 response.

A distinct pattern was observed for IL-8. LPS, mRNA 1, and mRNA 2 treatments all resulted in sustained IL-8 production over time, with levels close to the untreated control at 24 hours, followed by an increase at 48 hours and a decrease at 72 hours (Figure 8c). mRNA 1 showed the highest levels, suggesting significant and prolonged inflammation.

mRNA 2 induced a moderate increase in IL-8, similar to LPS.

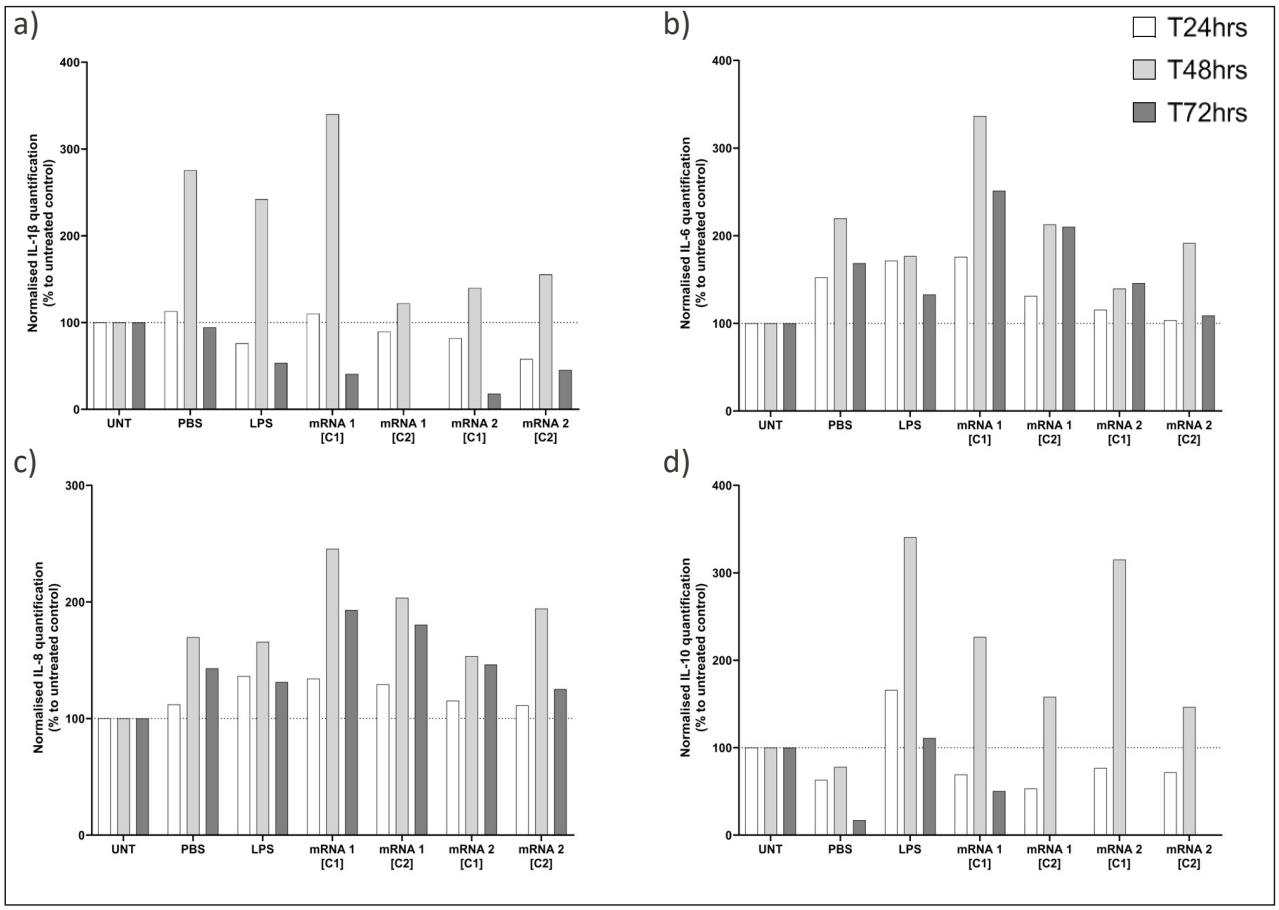

Figure 8. *Cytokines quantification on supernatants after injection:* 24h *(white)*, 48h *(light grey)*, 72h *(grey)*. *a)* IL1- β; *b)* IL-6; *c)* IL-8; *d)* IL-10. *The raw datas has been normalized to the untreated control.*

Analysis of IL-10, a key anti-inflammatory cytokine, revealed an increase in response to LPS at 24 hours, peaking at 48 hours and finally returning to a level close to the untreated control at 72 hours (Figure 8d).

For both mRNA formulations, we observed a response at 48 hours suggesting a late regulatory mechanism aimed at tempering the pro-inflammatory environment.

Collectively, these results indicate that mRNA 1 induces a delayed and longer pro-inflammatory response than the LPS control, while mRNA 2 exhibits a more moderate immune activation profile, potentially reflecting differences in formulation design.

4. Discussion

This study highlights the potential of 3D bioprinting a complex human skin model that includes muscle, adipose tissue, dermis, immune component, and epidermis. The high cell viability observed up to 31 days, as well as the functional differentiation of adipocytes and myocytes, confirm the compatibility of the bioinks used and the relevance of the 3D environment for maintaining specialised phenotypes. The tissue structure obtained, particularly at the dermo-epidermal junction, and the persistence of M1 macrophages highlight the interest of this model for the study of skin immune responses.

The integration of a standardised injection system made it possible to evaluate the impact of different mRNA formulations. The distinct metabolic and cytokine profiles observed between

two mRNA formulations highlight the model's ability to respond to external stimuli and its potential for screening injectable compounds.

In the future, the addition of additional immune cells (neutrophils, T-cells, B-cells, NK cells), endothelial cells for vascularization [4], and neuronal cells to simulate skin innervation will further expand the applications of this model. These improvements will pave the way for the development of an even more physiological multicellular systems, particularly suited to the needs of the cosmetics industry for evaluating the efficacy and tolerance of new active ingredients or formulations in an environment that closely mimics human skin.

5. Conclusion

Our research proves the feasibility and relevance of a multi-layered 3D bioprinted human skin model that includes differentiated and functional cell compartments, as well as an immune component. This model offers a robust and physiologically relevant platform for evaluating injectable formulations, particularly those based on mRNA. The marked differences between mRNAs formulations, both metabolically and immunologically, highlight the importance of evaluating the specific effects of each formulation in complex tissue environments. This system is a promising tool for preclinical screening of new therapeutic approaches targeting the skin and subcutaneous tissues, while limiting the use of animal experimentation.

6. Acknowledgments.

We would like to deeply thanks Natecia hospitals, Lyon, Clinique Saint-Vincent de Paul, Bourgoin-Jallieu, the doctors, nurses and donors of skin tissues for making possible the collection of skin and therefore the production of skin cells. We are also thankful to Ms Aurore Berton, Ms Jenily Xiong and Mr Corentin Barnier for technical help in the laboratory. We thank as well “La Région Auvergne-Rhône Alpes” and BPI France for supporting our 3D Bioprinting platform.

7. References

[1] Letsiou, S. Tracing skin aging process: a mini- review of in vitro approaches. Biogerontology 22, 261–272 (2021). https://doi.org/10.1007/s10522-021-09916-z.

[2] Shin SH, Lee YH, Rho N-K and Park KY(2023), Skin aging from mechanisms to interventions: focusing on dermal aging. Front. Physiol. doi: 10.3389/fphys.2023.1195272.

[3] Quílez, C et al,. Targeting the Complexity of In Vitro Skin Models: A Review of Cutting-Edge Developments. (2024). Journal of Investigative Dermatology, Volume 144, Issue 12. https://doi.org/10.1016/j.jid.2024.04.032.

[4] Colin McGuckin et al,. Linking Clinical Vascular Dark Circles Reduction to Laboratory In Vitro Modelization can be Achieved Using Vascularized 3D Bioprinted Skin Models. IFSCC Magazine journal, Volume 26 No 1.

[5] Lègues M et al,.The World’s First 3D Bioprinted Immune Skin Model Suitable for Screening Drugs and Ingredients for Normal and Inflamed Skin. IFSCC Magazine journal. Volume 23 | Number 4 | December 2020. 233-239 ISSN 1520-4561.